

# Numerical modelling of iron-pnictide bulk superconductor magnetization

Mark D Ainslie<sup>1</sup> , Akiyasu Yamamoto<sup>2,3</sup>, Hiroyuki Fujishiro<sup>4</sup>,  
Jeremy D Weiss<sup>5</sup> and Eric E Hellstrom<sup>6</sup>

<sup>1</sup> Bulk Superconductivity Group, Department of Engineering, University of Cambridge, Cambridge CB2 1PZ, United Kingdom

<sup>2</sup> Department of Applied Physics, Tokyo University of Agriculture and Technology, 2-24-16 Nakacho, Koganei, Tokyo 184-8588, Japan

<sup>3</sup> Materials Research Center for Element Strategy, Tokyo Institute of Technology, 4259 Nagatsuta, Midori, Yokohama, Kanagawa 226-8503, Japan

<sup>4</sup> Department of Physical Science and Materials Engineering, Faculty of Science and Engineering, Iwate University, Morioka 020-8551, Japan

<sup>5</sup> Department of Physics, University of Colorado, Boulder, CO 80309, United States of America

<sup>6</sup> Applied Superconductivity Center, National High Magnetic Field Laboratory, Florida State University, Tallahassee, FL 32310, United States of America

E-mail: [mark.ainslie@eng.cam.ac.uk](mailto:mark.ainslie@eng.cam.ac.uk)

Received 19 June 2017, revised 24 July 2017

Accepted for publication 4 August 2017

Published 5 September 2017



CrossMark

## Abstract

Iron-based superconductors exhibit a number of properties attractive for applications, including low anisotropy, high upper critical magnetic fields ( $H_{c2}$ ) in excess of 90 T and intrinsic critical current densities above  $1 \text{ MA cm}^{-2}$  (0 T, 4.2 K). It was shown recently that bulk iron-pnictide superconducting magnets capable of trapping over 1 T (5 K) and 0.5 T (20 K) can be fabricated with fine-grain polycrystalline  $\text{Ba}_{0.6}\text{K}_{0.4}\text{Fe}_2\text{As}_2$  (Ba122). These Ba122 magnets were processed by a scalable, versatile and low-cost method using common industrial ceramic processing techniques. In this paper, a standard numerical modelling technique, based on a 2D axisymmetric finite-element model implementing the  $\mathbf{H}$ -formulation, is used to investigate the magnetisation properties of such iron-pnictide bulk superconductors. Using the measured  $J_c(B, T)$  characteristics of a small specimen taken from a bulk Ba122 sample, experimentally measured trapped fields are reproduced well for a single bulk, as well as a stack of bulks. Additionally, the influence of the geometric dimensions (thickness and diameter) on the trapped field is analysed, with a view of fabricating larger samples to increase the magnetic field available from such trapped field magnets. It is shown that, with current state-of-the-art superconducting properties, surface trapped fields  $>2 \text{ T}$  could readily be achieved at 5 K (and  $>1 \text{ T}$  at 20 K) with a sample of diameter 50 mm. Finally, an aspect ratio of between 1 and 1.5 for  $R/H$  (radius/thickness) would be an appropriate compromise between the accessible, surface trapped field and volume of superconducting material for bulk Ba122 magnets.

Keywords: bulk superconductors, critical current density (superconductivity), finite-element method, iron pnictides, numerical simulation, trapped field magnets

(Some figures may appear in colour only in the online journal)

## 1. Introduction

The discovery of superconductivity in iron-pnictide compounds in 2008 [1] raised the prospect of finding high-temperature

superconductivity in materials other than cuprates and a great deal of research has been carried out towards practical implementation in thin film, wire and bulk forms. Bulk superconducting materials, in particular, can be used as super-strength,

trapped field magnets (TFMs) and magnetic fields greater than 17 T [2] have been achieved in large, single-grain (RE)BCO (where RE = rare earth or Y) bulk superconductors. This makes them attractive for a number of engineering applications that rely on high magnetic fields, including compact and energy-efficient electrical machines, magnetic separation and magnetic drug delivery systems.

The iron-based superconductors exhibit a number of properties attractive for applications, including low anisotropy, high upper critical magnetic fields ( $H_{c2}$ ) in excess of 90 T and intrinsic critical current densities above  $1 \text{ MA cm}^{-2}$  (0 T, 4.2 K). It was shown recently in [3] that bulk iron-pnictide superconducting magnets capable of trapping over 1 T (5 K) and 0.5 T (20 K) can be fabricated with fine-grain polycrystalline  $\text{Ba}_{0.6}\text{K}_{0.4}\text{Fe}_2\text{As}_2$  (Ba122). These Ba122 magnets were processed by a scalable, versatile and low-cost method using common industrial ceramic processing techniques.

In this paper, a standard numerical modelling technique, based on a 2D axisymmetric finite-element model implementing the  $\mathbf{H}$ -formulation, is used to investigate the magnetisation properties of such iron-pnictide bulk superconductors. Using the measured  $J_c(B, T)$  characteristics of small specimens taken from bulk Ba122 samples, the experimentally measured trapped fields in [3] are reproduced to good effect. Additionally, the influence of the geometric dimensions (thickness and diameter) on the trapped field is analysed, with a view of fabricating larger samples to increase the magnetic field available from such TFMs.

## 2. Modelling framework and verification

### 2.1. Sample information

To fabricate the bulk Ba122 samples investigated in this study, as described in [3], Ba, K, Fe, and As in a molar ratio of 0.6:0.42:2:2 were reacted together by a mechanochemical reaction, followed by sintering in a hot isostatic press (HIP) at  $600^\circ\text{C}$  using a procedure described elsewhere in [4]. After bulk synthesis and subsequent re-milling, approximately 3–5 g of Ba122 powder was pressed into 15.9 mm diameter pellets and then further densified in a cold isostatic press at 276 MPa. These were then wrapped with Ag foil and inserted into a steel tube that was carefully machined to the diameter of the pellet and foil. Both ends of the steel tube were welded shut under vacuum using chamfered plugs that helped the steel tube to compress the pellet. After welding, the tubes were swaged and cold isostatically pressed to further shape and densify them, reducing the diameter of the samples approximately 10%. Finally, the samples were sintered for 10 h at  $600^\circ\text{C}$  in the HIP. After heat treatment, the steel tubes were sliced with a diamond saw to reveal the pellet surfaces.

### 2.2. Modelling framework

Figure 1 shows the 2D axisymmetric models used in this paper to simulate the magnetisation of iron-pnictide (Ba122)

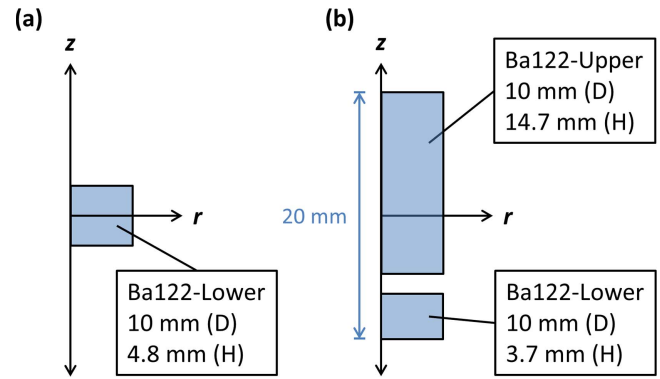


**Figure 1.** 2D axisymmetric models for numerical simulation of iron-pnictide (Ba122) bulk superconductors. (a) Single Ba122 bulk, ‘Ba122-Lower,’ of diameter (D) 10 mm and thickness (H) 4.8 mm, and (b) stack of Ba122 bulks, comprising the same ‘Ba122-Lower’ bulk from (a), but polished to a thickness of 3.7 mm, and an upper bulk, ‘Ba122-Upper,’ comprised of bulks of diameter 10 mm and totalling thickness 14.7 mm. A 1.6 mm spacer (not modelled) exists between the two bulks to accommodate a Hall sensor, as described in [3].

bulk superconductors. The model shown in figure 1(b) represents experimental setup for the bulk Ba122 magnet stack measured in [3], and figure 1(a) shows the single lower bulk, ‘Ba122-Lower,’ in this stack before it was machined to the thickness of 3.7 mm.

The electromagnetic properties are simulated using the 2D axisymmetric  $\mathbf{H}$ -formulation, implemented in the commercial software package COMSOL Multiphysics 5.2a and used previously by the authors to simulate bulk high-temperature superconductors [5–9], as well as bulk  $\text{MgB}_2$  [10]. Isothermal conditions are assumed because the magnetisation process is slow; hence, no thermal model is included. The governing equations are derived from Maxwell’s equations—namely, Faraday’s (1) and Ampere’s (2) laws:

$$\nabla \times \mathbf{E} + \left( \frac{d\mathbf{B}}{dt} \right) = \nabla \times \mathbf{E} + \frac{d(\mu_0 \mu_r \mathbf{H})}{dt} = 0, \quad (1)$$

$$\nabla \times \mathbf{H} = \mathbf{J}, \quad (2)$$

where  $\mu_0$  is the permeability of free space, and for the superconducting and surrounding sub-domains, the relative permeability is simply  $\mu_r = 1$ .

The results of the model depend strongly on the in-field, temperature-dependent critical current density,  $J_c(B, T)$ , of the superconducting material [11], and the experimental data for  $J_c(B)$  of a small specimen taken from the lower bulk, ‘Ba122-Lower,’ measured at 4.2, 10, 20 and 25 K in fields up to 10 T is shown in figure 2 (solid lines). Estimated  $J_c(B)$  characteristics for the upper bulk, ‘Ba122-Upper,’ are also included in figure 2 (dashed lines), which are estimated from remnant trapped field data that suggested a self-field  $J_c$ , i.e. average, in-field  $J_c$ , of around  $41.1 \text{ kA cm}^{-2}$  (compared to  $74 \text{ kA cm}^{-2}$  for the lower sample). It is assumed that the upper bulk has the same field dependence as the lower one, but such that  $J_c$  is always  $41.1/74$  of the lower one.

The  $J_c(B, T)$  data is input into the model using a two-variable, direct interpolation, as described in [12, 13] to

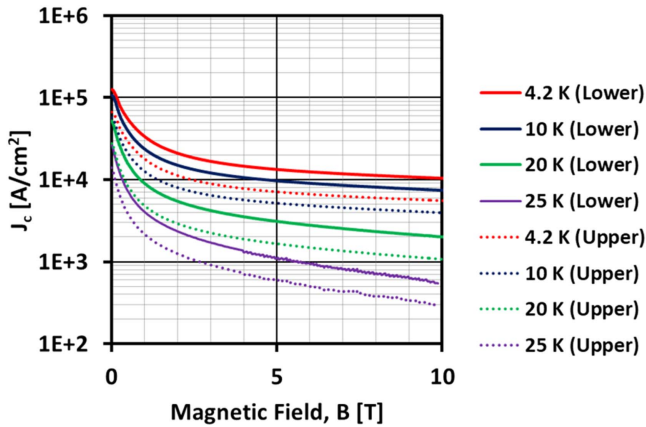


**Figure 2.**  $J_c(B, T)$  characteristics for a small specimen taken from the lower bulk, ‘Ba122-Lower,’ in figure 1(b) measured at 4.2, 10, 20 and 25 K in fields up to 10 T (solid lines). Estimated  $J_c(B)$  characteristics for the upper bulk, ‘Ba122-Upper,’ are also included (dashed lines), which are estimated from the remnant trapped field data.

implement the complex  $J_c(B, \theta)$  behaviour of high-temperature superconducting (HTS) coated conductors and as used in [8, 9] to simulate the  $J_c(B, T)$  properties of a bulk Gd-Ba-Cu-O superconductor. A key advantage of this modelling technique is that it is flexible to include different materials and different superconducting properties, and it can predict trapped fields with good accuracy, despite the fact that the upper and lower bulks have different  $J_c$  characteristics. This variation in  $J_c$  was observed experimentally between the two separate batches from which the samples came from, but little variation was seen between samples within each particular batch.

The  $E$ - $J$  power law ( $E \propto J^n$ ) [14, 15] is used to simulate the nonlinear electrical resistivity of the superconductor, where  $n = 50$  and  $E_0 = 1 \times 10^{-4} \text{ V m}^{-1}$ . It should be noted that the  $n$  value is higher than that used commonly for HTS materials, since the observed flux creep in the Ba122 bulks is comparatively much weaker (see figure 4 in [3], for example, where the trapped field at 5 K decayed approximately only 3% after one day). Such a high  $n$  value also gives a good approximation of critical state models.

To simulate the field-cooled (FC) magnetisation process as carried out experimentally in [3], a zero-field-cooled (ZFC) magnetisation process is employed in the simulations by applying a large, slowly-ramped external magnetic field that is several times larger than the full penetration field of the bulk. By setting appropriate boundary conditions, a uniform background magnetising field is ramped from 0 to 5 T at  $1.5 \text{ T min}^{-1}$ , then ramped back to 0 T at the same rate. After waiting +10 min for relaxation of the trapped field, the magnetic flux density is then calculated at locations corresponding to the approximate location of the Hall sensors used to take the experimental measurements, which will be specified in the following sections.

### 2.3. Single Ba122 bulk

Figure 3 shows a comparison of the experimental and numerical simulation results for the single Ba122 bulk,

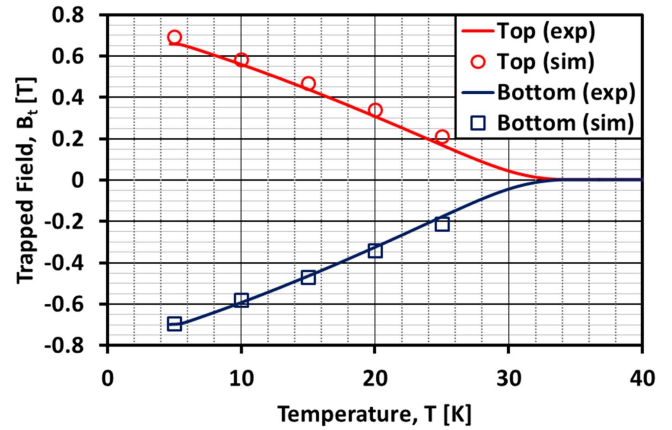


**Figure 3.** Comparison of experimental (solid lines) and numerical simulation (symbols) results for the single Ba122 bulk, ‘Ba122-Lower,’ shown in figure 1(a) and using the measured  $J_c(B)$  data shown in figure 2.

‘Ba122-Lower’ (shown in figure 1(a)). For the experimental measurement, the bulk is FC (applied field,  $B_{\text{app}} = 6 \text{ T}$ ) to approximately 5 K, with the field subsequently reduced to zero, followed by increasing the temperature at a rate of  $0.5 \text{ K min}^{-1}$ . Hall sensors located at the centre of the top and bottom surfaces of the bulk measured the magnetic field density,  $B_z$ .

In the numerical simulations, the trapped magnetic field,  $B_t$ , is calculated at  $t = +10 \text{ min}$  after the application and removal of the magnetising field, at  $z = +2.9 \text{ mm}$ ,  $r = 0 \text{ mm}$  and  $z = -2.9 \text{ mm}$ ,  $r = 0 \text{ mm}$ , corresponding to the top and bottom Hall sensor locations, respectively (the surfaces of the bulk are located at  $\pm 2.4 \text{ mm}$ ). The simulation results are given for discrete points between 5 and 25 K at increments of 5 K, within the range of the input  $J_c(B)$  data detailed in the previous section.

The simulations reproduce the experimental results very well, validating the model assumptions, and since the results are reproduced using only a single, small specimen taken from the bulk, this suggests the sample has a homogeneous  $J_c$  distribution on a macroscopic scale, like bulk  $\text{MgB}_2$  [17] and in contrast to the inhomogeneous  $J_c$  distribution that can occur during the growth of  $c$ -axis seeded, single-grain (RE)BCO bulk superconductors [18]. Nonetheless, it should be noted that pulsed field magnetisation is a more useful tool for highlighting the inhomogeneity of the  $J_c$  distribution in a bulk superconductor than FC magnetisation [19].

### 2.4. Stack of Ba122 bulks

Figure 4 shows a comparison of the experimental (as presented in [3]) and numerical simulation results for the stack of Ba122 bulks. This stack comprises the same ‘Ba122-Lower’ bulk analysed in section 2.3, but polished to a thickness of 3.7 mm, and an upper bulk, ‘Ba122-Upper,’ of diameter 10 mm and thickness 14.7 mm. A 1.6 mm spacer (not modelled) exists between the two bulks to accommodate a Hall sensor.

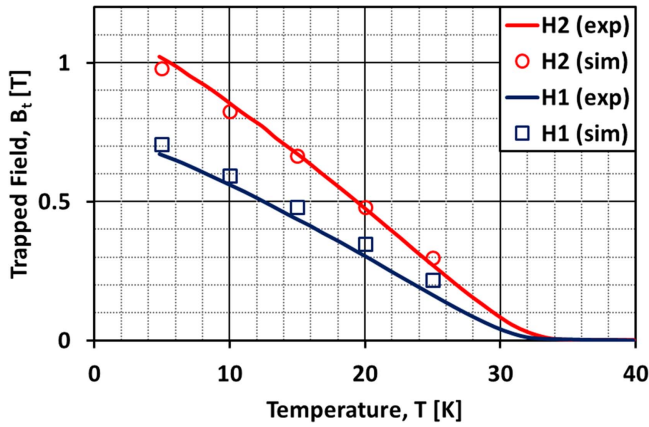


**Figure 4.** Comparison of experimental [3] and numerical simulation results for the stack Ba122 of bulks shown in figure 1(b) and using the measured and estimated  $J_c(B)$  data shown in figure 2.

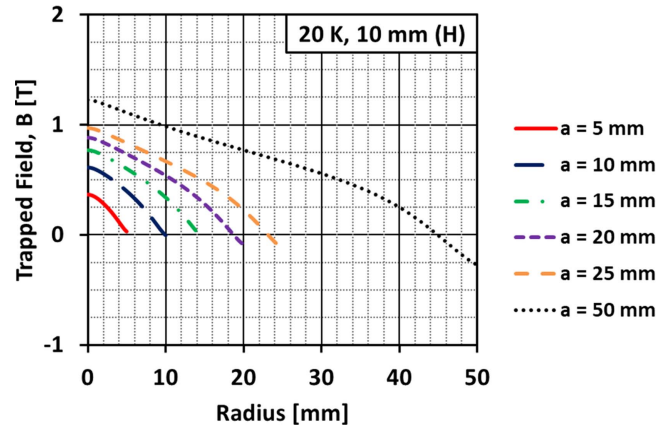


**Figure 7.** Numerical simulation results for diameter dependence of the trapped field across the top surface ( $z = +0.5$  mm) of the Ba122 bulk with fixed thickness,  $H$ , of 10 mm, for an operating temperature of 20 K. The  $B(r = 0$  mm) values correspond to the values given in figure 5.

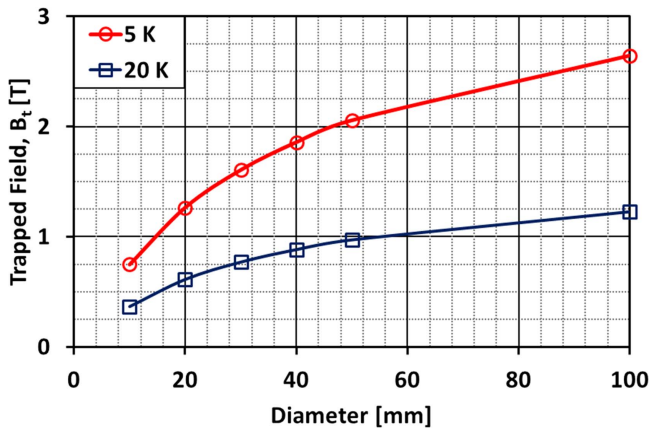


**Figure 5.** Numerical simulation results for the diameter dependence of the trapped field at  $r = 0$  mm,  $z = +0.5$  mm above the top surface,  $B_t$ , of the Ba122 bulk with fixed thickness,  $H$ , of 10 mm, for operating temperatures of 5 and 20 K. The measured  $J_c(B, T)$  characteristics of ‘Ba122-lower’ presented in section 2.2 are assumed.

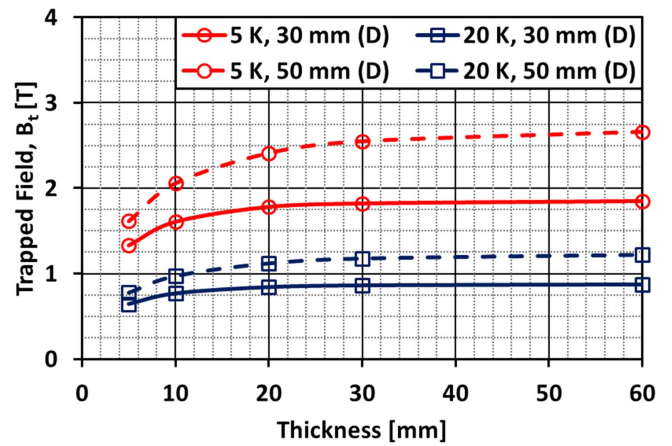


**Figure 8.** Numerical simulation results for the thickness dependence of the trapped field at  $r = 0$  mm,  $z = +0.5$  mm above the top surface,  $B_t$ , of the Ba122 bulk with fixed diameters,  $D$ , of 30 and 50 mm, for operating temperatures of 5 and 20 K. The measured  $J_c(B, T)$  characteristics of ‘Ba122-lower’ presented in section 2.2 are assumed.

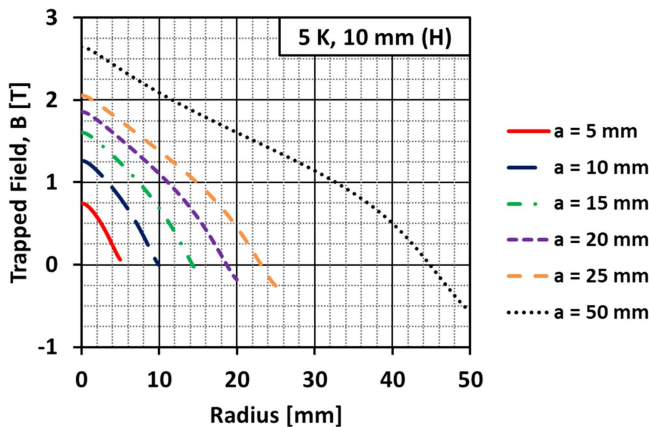


**Figure 6.** Numerical simulation results for diameter dependence of the trapped field across the top surface ( $z = +0.5$  mm) of the Ba122 bulk with fixed thickness,  $H$ , of 10 mm, for an operating temperature of 5 K. The  $B(r = 0$  mm) values correspond to the values given in figure 5.

For the experimental measurement, the bulk is FC ( $B_{app} = 8$  T) to approximately 5 K, with the field subsequently reduced to zero, followed by increasing the temperature at a rate of  $0.2$  K  $\text{min}^{-1}$  [3]. Hall sensors located at the centre of the 1.6 mm spacer in between the upper and lower bulks (labelled H2) and at the centre of the bottom surface of the lower bulk (labelled H1) measured the magnetic field density,  $B_z$  [3].

In the numerical simulations, the trapped magnetic field,  $B_t$ , is calculated  $t = +10$  min after the application and removal of the magnetising field, at  $z = -5.5$  mm,  $r = 0$  mm and  $z = -10.5$  mm,  $r = 0$  mm, corresponding to these Hall sensor locations. As per the previous section, the simulation results are given for discrete points between 5 and 25 K at increments of 5 K, within the range of the input  $J_c(B)$  data. Again, the simulations reproduce the experimental results well, and there is of course scope for improvement of the accuracy of the simulation by using a more exact, measured

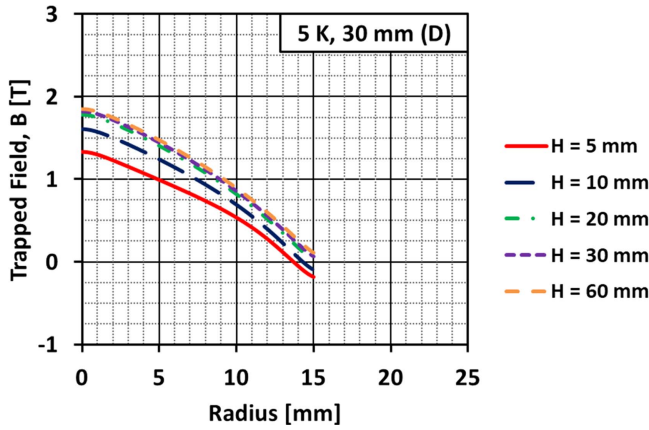


**Figure 9.** Numerical simulation results for thickness dependence of the trapped field across the top surface ( $z = +0.5$  mm) of the Ba122 bulk with fixed diameter,  $D$ , of 30 mm, for an operating temperature of 5 K. The  $B(r = 0$  mm) values correspond to the values given in figure 8.

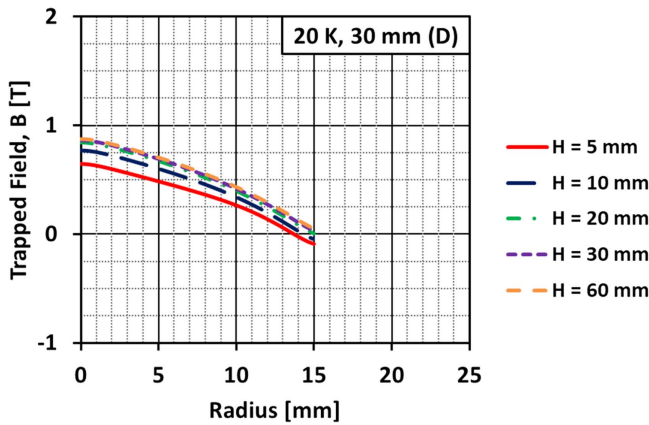


**Figure 10.** Numerical simulation results for thickness dependence of the trapped field across the top surface ( $z = +0.5$  mm) of the Ba122 bulk with fixed diameter,  $D$ , of 30 mm, for an operating temperature of 20 K. The  $B(r = 0$  mm) values correspond to the values given in figure 8.

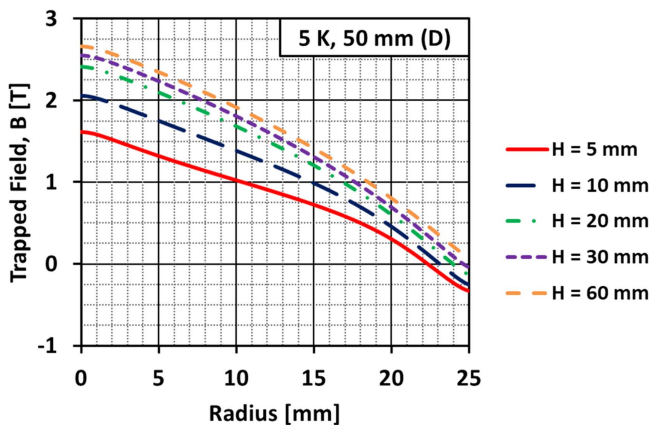


**Figure 11.** Numerical simulation results for thickness dependence of the trapped field across the top surface ( $z = +0.5$  mm) of the Ba122 bulk with fixed diameter,  $D$ , of 50 mm, for an operating temperature of 5 K. The  $B(r = 0$  mm) values correspond to the values given in figure 8.

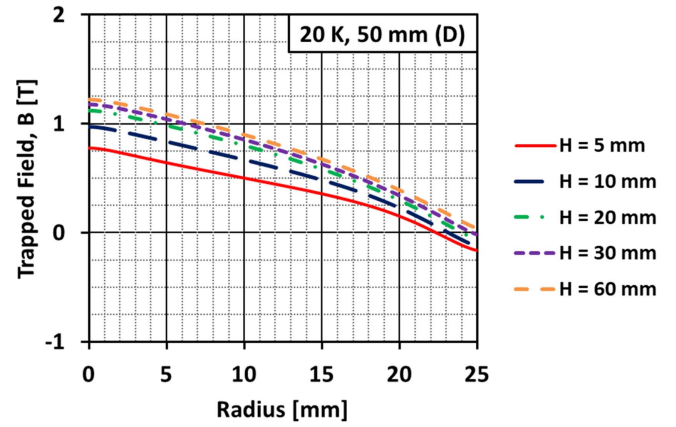


**Figure 12.** Numerical simulation results for thickness dependence of the trapped field across the top surface ( $z = +0.5$  mm) of the Ba122 bulk with fixed diameter,  $D$ , of 50 mm, for an operating temperature of 20 K. The  $B(r = 0$  mm) values correspond to the values given in figure 8.

$J_c(B, T)$  characteristic for the upper bulk, rather than the estimation described in section 2.2. Nevertheless, the simulations are a useful tool to estimate the trapped field in such bulks or stacks of bulks. In the next section, the influence of the geometric dimensions (thickness and diameter) on the trapped field is analysed, with a view of fabricating larger samples to increase the magnetic field, since their fabrication is scalable, versatile, low-cost and based on common industrial ceramic processing techniques.

### 3. Influence of geometric parameters

Using the numerical model and the same assumptions for the superconducting properties, the trapped field of larger Ba122 samples can be predicted without the need for further experiments. In this section, the measured ‘Ba122-Lower’  $J_c(B, T)$  characteristics presented in section 2.2 are assumed and an analysis of the diameter and thickness dependence of the trapped field is carried out for different sample sizes.

#### 3.1. Fixed thickness, diameter variation

Figure 5 shows the diameter dependence of the trapped field at  $r = 0$  mm,  $z = +0.5$  mm above the top surface,  $B_t$ , of the Ba122 bulk with a fixed thickness,  $H$ , of 10 mm, for operating temperatures of 5 and 20 K. Figures 6 and 7 show the trapped field across the top surface (again at  $z = +0.5$  mm) for 5 and 20 K, respectively, where  $B(r = 0$  mm) corresponds to the value given in figure 5. As per section 2, the  $B_t$  value is given for  $t = +10$  min after the application and removal of the magnetising field. The trapped field increases with increasing sample diameter and the rate of increase decreases with diameter. This occurs for two reasons: firstly, from Bean’s critical state model as applied to a thin disc-shaped bulk (3):

$$B_t = k\mu_0 J_c R, \quad (3)$$

where  $R = D/2$  is the sample radius and  $k$  is a correction factor to the simple Bean (slab) approximation due to the

finite thickness,  $H$ , of a disc-shaped bulk superconductor sample, given by

$$k = \frac{H}{2R} \ln \left( \frac{R}{H} + \sqrt{1 + \left( \frac{R}{H} \right)^2} \right). \quad (4)$$

It can be seen that the correction factor  $k$  decreases with increasing aspect ratio, which reduces the trapped field, but  $J_c$  also reduces with increasing diameter because of the larger magnetic field generated from the supercurrent flowing over a larger area. In contrast with  $\text{MgB}_2$  bulks, whose  $J_c(B)$  characteristics follow an exponential law that can decrease rapidly in field [10], rapid saturation of  $B_t$  is not observed for the Ba122 bulks with increasing diameter. Enhancing the pinning to improve the  $J_c(B, T)$  characteristics is another obvious route to increasing the trapped field; however, the simulation results suggest that, based on current superconducting properties, surface trapped fields  $>2$  T could readily be achieved at 5 K (and  $>1$  T at 20 K) with a sample of diameter 50 mm.

In the following subsection, we investigate the thickness dependence of the trapped field for fixed diameters,  $D$ , of 30 and 50 mm, which are typical sizes of practical bulk high-temperature superconductors.

### 3.2. Fixed diameter, thickness variation

Figure 8 shows the thickness dependence of the trapped field at  $r = 0$  mm,  $z = +0.5$  mm above the top surface,  $B_t$ , of the Ba122 bulk with fixed diameters,  $D$ , of 30 and 50 mm, for operating temperatures of 5 and 20 K. Figures 9–12 show the trapped field across the top surface (again at  $z = +0.5$  mm) for 5 and 20 K for  $D = 30$  mm (figures 9 and 10) and  $D = 50$  mm (figures 11 and 12). The trapped field saturates as the thickness,  $H$ , of the bulk approaches  $D$ , which can be deduced from (3) and (4), and is observed for bulk (RE)BCO superconductors [20], as well as bulk  $\text{MgB}_2$  [10]. From these results, the geometry of the bulk can be optimised, and as found in [21] for bulk (RE)BCO superconductors, an aspect ratio of between 1 and 1.5 for  $R/H$  (radius/thickness) would also be an appropriate compromise between the accessible, surface trapped field and volume of superconducting material for bulk Ba122 magnets.

## 4. Conclusion

In this paper, a 2D axisymmetric finite-element model implementing the  $H$ -formulation is used to investigate the magnetisation properties of iron-pnictide (Ba122) bulk superconductors. Using the measured  $J_c(B, T)$  characteristics of a small specimen taken from a bulk Ba122 sample, experimentally measured trapped fields are reproduced well for a single bulk, as well as a stack of bulks. The influence of the geometric dimensions (thickness and diameter) on the trapped field was then analysed, with a view of fabricating larger samples to increase the magnetic field available from such TFMs. It is shown that, with current state-of-the-art superconducting properties, surface trapped fields  $>2$  T could

readily be achieved at 5 K (and  $>1$  T at 20 K) with a sample of diameter 50 mm. Finally, an aspect ratio of between 1 and 1.5 for  $R/H$  (radius/thickness) would be an appropriate compromise between the accessible, surface trapped field and volume of superconducting material for bulk Ba122 magnets.

## Acknowledgments

Mark Ainslie would like to acknowledge financial support from a Royal Academy of Engineering Research Fellowship. Hiroyuki Fujishiro would like to acknowledge financial support from JSPS KAKENHI Grant No. 15K04646. The work at NHMFL was supported NSFDMR-1306785, by the National High Magnetic Field Laboratory, which is supported by the National Science Foundation under NSFDMR-1157490, and by the State of Florida. The work at TUAT was supported by MEXT Elements Strategy Initiative to Form Core Research Center and by JSPS KAKENHI Grant No. JP15H05519.

## ORCID iDs

Mark D Ainslie  <https://orcid.org/0000-0003-0466-3680>

## References

- [1] Kamihara Y, Watanabe T, Hirano M and Hosono H 2008 Iron-based layered superconductor  $\text{La}[\text{O}_{1-x}\text{F}_x]\text{FeAs}$  ( $x = 0.05\text{--}0.12$ ) with  $T_c = 26$  K *J. Am. Chem. Soc.* **130** 3296–7
- [2] Durrell J H *et al* 2014 A trapped field of 17.6 T in melt-processed, bulk Gd-Ba-Cu-O reinforced with shrink-fit steel *Supercond. Sci. Technol.* **27** 082001
- [3] Weiss J D *et al* 2015 Demonstration of an iron-pnictide bulk superconducting magnet capable of trapping over 1 T *Supercond. Sci. Technol.* **28** 112001
- [4] Weiss J D, Jiang J, Polyanskii A A and Hellstrom E E 2013 Mechanochemical synthesis of pnictide compounds and superconducting  $\text{Ba}_{0.6}\text{K}_{0.4}\text{Fe}_2\text{As}_2$  bulks with high critical current density *Supercond. Sci. Technol.* **26** 074003
- [5] Zou J, Ainslie M D, Hu D and Cardwell D A 2015 Influence of time-varying external magnetic fields on trapped fields in bulk superconductors *IEEE Trans. Appl. Supercond.* **25** 4900505
- [6] Philippe M P *et al* 2015 Influence of soft ferromagnetic sections on the magnetic flux density profile of a large grain, bulk Y-Ba-Cu-O superconductor *Supercond. Sci. Technol.* **28** 095008
- [7] Zou J, Ainslie M D, Hu D and Cardwell D A 2016 Mitigation of demagnetization of bulk superconductors by time-varying external magnetic fields *IEEE Trans. Appl. Supercond.* **26** 8200605
- [8] Ainslie M D *et al* 2016 Enhanced trapped field performance of bulk high-temperature superconductors using split coil, pulsed field magnetization with an iron yoke *Supercond. Sci. Technol.* **29** 074003
- [9] Ainslie M D *et al* 2016 Flux jump-assisted pulsed field magnetisation of high- $J_c$  bulk high-temperature superconductors *Supercond. Sci. Technol.* **29** 124004

- [10] Zou J *et al* 2015 Numerical modelling and comparison of MgB<sub>2</sub> bulks fabricated by HIP and infiltration growth *Supercond. Sci. Technol.* **28** 075009
- [11] Dew-Hughes D 2001 The critical current of superconductors: an historical review *Low Temp. Phys.* **27** 713–22
- [12] Hu D *et al* 2015 DC characterization and 3D modelling of a triangular, epoxy-impregnated high temperature superconducting coil *Supercond. Sci. Technol.* **28** 065011
- [13] Hu D *et al* 2016 Modeling and comparison of in-field critical current density anisotropy in high-temperature superconducting (HTS) coated conductors *IEEE Trans. Appl. Supercond.* **26** 6600906
- [14] Plummer C J G and Evetts J E 1987 Dependence of the shape of the resistive transition on composite inhomogeneity in multifilamentary wires *IEEE Trans. Magn.* **23** 1179–82
- [15] Rhyner J 1993 Magnetic properties and AC-losses of superconductors with power law current–voltage characteristics *Physica C* **212** 292–300
- [16] Ainslie M D and Fujishiro H 2015 Modelling of bulk superconductor magnetization *Supercond. Sci. Technol.* **28** 053002
- [17] Yamamoto A, Ishihara A, Tomita M and Kishio K 2014 Permanent magnet with MgB<sub>2</sub> bulk superconductor *Appl. Phys. Lett.* **105** 032601
- [18] Ainslie M D *et al* 2014 Modelling and comparison of trapped fields in (RE)BCO bulk superconductors for activation using pulsed field magnetization *Supercond. Sci. Technol.* **27** 065008
- [19] Fukai H *et al* 2005 The effect of inhomogeneous flux penetration into bulk superconductor by pulsed field magnetization *Supercond. Sci. Technol.* **18** 1179–82
- [20] Fukai H, Tomita M, Murakami M and Nagamoto T 2002 The effect of geometry on the trapped magnetic field in bulk superconductors *Supercond. Sci. Technol.* **15** 1054–7
- [21] Eisterer M *et al* 2006 Limitations for the trapped field in large grain YBCO superconductors *Supercond. Sci. Technol.* **19** S530–6